# Proton decay following the transfer reaction ($^{7}$Li, $^{6}$He) on $^{40}$Ca and $^{90}$Zr

G. H. Yoo,* G. M. Crawley,† J. H. Kelley,‡ N. A. Orr,§ J. C. Staško,‖ and J. S. Winfield¶
*National Superconducting Cyclotron Laboratory and Department of Physics & Astronomy, Michigan State University, East Lansing, Michigan 48824*

S. Galès, S. Fortier, H. Laurent, and T. Suomijärvi
*Institut de Physique Nucléaire, CNRS-IN2P3, F-91406 Orsay, France*

J. E. Finck
*Physics Department, Central Michigan University, Mt. Pleasant, Michigan 48859*
(Received 7 December 1999; published 1 September 2000)

The charged particle decay of continuum states excited by the single proton stripping reaction ($^{7}$Li, $^{6}$He) at a bombarding energy of 50 MeV/nucleon on targets of $^{40}$Ca and $^{90}$Zr was measured and compared with theoretical predictions. The results suggest that most of the strength in the continuum arises from decay of unbound states in the intermediate nucleus rather than from breakup of the $^{7}$Li projectile. There is substantial direct decay to the low-lying states in the final nucleus for both targets.

PACS number(s): 25.70.Hi, 23.20.En, 24.60.−k

## I. INTRODUCTION

A continuum, usually considered a ''background,'' is often observed at high excitation energy in single nucleon stripping reactions [1]. This continuum makes it difficult to extract information about the states observed as broad resonancelike structures at high excitation energy. In many cases, the continuum is assumed to arise from breakup processes and is simply regarded as an uninteresting and unwanted complication to be subtracted empirically from the spectrum. The present experiment is designed to separate the cross section due to resonance states from the breakup processes by detection of decay protons at backward angles in coincidence with ejectiles at zero degrees. In addition, the coincidence measurements will permit an investigation of the damping of these resonance states by comparison with a statistical decay model, thus determining the direct component of their decay.

A recent semiclassical approach developed by Bonaccorso and Brink [2–5] (BB) has attempted to calculate the strength from both breakup and resonance absorption in the continuum in a unified manner. This approach treats the process of breakup of the projectile and capture of a nucleon into an unbound state simultaneously and has been quite successful in explaining the energy dependence of the inclusive cross section for a number of neutron-transfer reactions induced by heavy ions [6]. The model predicts that for many heavy-ion induced neutron-transfer reactions at bombarding energies above 20 MeV/nucleon, a significant amount of the strength in the continuum arises from capture into resonances which subsequently decay by particle emission. Unfortunately the BB model has not yet been extended to charged-particle transfer reactions. However, in proton transfer on a number of targets [7], broad peaks are also observed above an underlying continuum and, particularly at excitation energies where the proton decay energy is above the Coulomb barrier, similar results to those predicted in neutron transfer are expected. This experiment attempts to test such predictions on two medium-weight targets.

Breakup processes can be divided into two broad categories, elastic breakup and inelastic breakup. In the elastic breakup process, the projectile fragments because of its interaction with the target nucleus while leaving the target in its ground state. Both fragments from the original projectile move along a path similar to the extension of the projectile's path and are therefore emitted preferentially at forward angles. In an inelastic breakup process, the target can be excited. In general, the distribution of particles from inelastic breakup will also be peaked at forward angles, whereas the decay from resonant states will be symmetric about 90° in the center of mass of the decaying nucleus. In the BB model, elastic breakup is defined as breakup without any interaction in the final state between the projectile and the target potential. The absorption process, associated with the imaginary part of the nucleon-target optical potential, involves a final-state interaction and includes both resonance absorption and inelastic breakup. The relative strength of the elastic and inelastic breakup processes depends upon the relative strength of the real and imaginary parts of the optical potential used in the BB model and thus depends on the details of the reaction including the bombarding energy.

The decay of resonance states can proceed either by a direct process or a statistical process. If the resonance states

*Present address: Department of Electrical Engineering, Dae Bul University, Sam-Ho Myun, Young-Arm Kun, South Korea.
†Present address: College of Science and Mathematics, University of South Carolina, Columbia, SC 29208.
‡Present address: Department of Physics, Duke University, Durham, NC 27708.
§Present address: Laboratoire de Physique Corpusculaire, IN2P3-CNRS, ISMRA et Université de Caen, 14050 Caen cedex, France.
¶Present address: Advanced Power Source Technology, Ford Motor Company, Dearborn, MI 48121.
‖Present address: Laboratori Nazionali del Sud–INFN, via S. Sofia, 44-95123 Catania, Italy.

 

are fully damped, their decay should be predicted by statistical decay calculations. Departures from such predictions will identify direct decay of the resonance states. In addition, the angular distributions of the decay protons may provide information on the spin parity of the decaying resonance states. Finally, the direct decay, particularly for high-lying states, should provide some indication of the parentage of these states.

Specifically, the present experiment explores the nature of the underlying continuum in the case of the reaction ($^7$Li, $^6$He) at 50 MeV/nucleon on $^{40}$Ca and $^{90}$Zr by observing the proton decay of states in $^{41}$Sc and $^{91}$Nb above the proton emission threshold. This reaction is known to populate broad resonance states in a variety of targets [7] and the $^6$He ejectile has no particle-stable excited states to complicate the residual spectra. The targets were chosen because they had low-energy thresholds for proton emission and comparatively high neutron emission thresholds. The $^6$He particles were detected near zero degrees in coincidence with the charged particles emitted at backward angles. This technique is expected to select states which arise from capture into resonance states of the target plus a single proton, and to exclude particles resulting from elastic breakup which will be emitted at forward angles. This assumption was checked by placing one proton detector at 32° to monitor the symmetry of the angular correlation, since breakup processes will show a maximum towards forward angles.

## II. EXPERIMENTAL PROCEDURE

The $^7$Li projectiles were accelerated to 50 MeV/nucleon by the K1200 superconducting cyclotron at Michigan State University. For the $^{40}$Ca target, natural calcium metal (96.94% $^{40}$Ca) was rolled to a thickness of 4.4 mg/cm$^2$. The $^{90}$Zr target was enriched to 98.7% and was 5.1 mg/cm$^2$ thick. The $^6$He ejectiles were detected around zero degrees in the focal plane of the A1200 beam analyzer system [8], the second half of which was used as a magnetic spectrograph with an angular acceptance of 4 msr. This restricted the detection of $^6$He particles to a maximum angle of two degrees. The ability of this system to detect cleanly the $^6$He particles at small angles close to zero degrees simplified the analysis of the experiment because the recoil direction of the intermediate heavy ion is therefore constrained also to be close to zero degrees. The focal plane detectors consisted of two position sensitive silicon detectors (1 mm thick, 1 cm high, and 5 cm long) one behind the other and separated by 1 cm, and followed by a plastic scintillator. The particles detected in the focal plane were identified by energy loss in the two position sensitive detectors, total energy in the plastic scintillator and time of flight between the plastic scintillator and the beam pulse. The energy resolution for the $^6$He spectra was about 500 keV full width at half maximum.

An array of eight silicon detectors, each of 5 cm$^2$ area and 5 mm thick were arranged to detect charged particles in coincidence with the $^6$He particles in the focal plane, and to measure the angular correlation, $W(\theta)$. Thin aluminized Mylar foils of thickness about 25 $\mu$m were placed in front of the silicon detectors to stop low-energy electrons from the target reaching the detectors. Each of the silicon detectors in the array was located approximately 14 cm from the target. Seven silicon detectors were placed at backward angles in the range of $161° \geqslant \theta \geqslant 110°$, and the eighth at $\theta = 32°$. The total solid angle of the silicon detector array was 0.20 sr. This system allowed the detection of charged particles, but did not permit the identification of the particle type. However, since the Coulomb barrier for $\alpha$ particles is twice the barrier for protons, very few $\alpha$ particles are expected to be emitted. In addition, deuterons are not expected throughout most of the energy region of interest because their threshold energy is significantly (typically 10 MeV) higher than the energy threshold for proton emission. These qualitative expectations were confirmed by calculations with the program CASCADE [9], which uses Hauser-Feshbach theory, and predicts very limited $\alpha$ or deuteron emission in the excitation energy range of interest in the nuclei studied in this experiment.

The energy calibration of the focal plane was carried out using elastic scattering from a $^{12}$C target. For the calibrations, the elastically scattered particles from $^{12}$C were moved across the focal plane by varying the magnetic field of the dipole magnet. The silicon detector array was energy calibrated using the $^{12}$C($^7$Li, $^6$He)$^{13}$N reaction and observing the decay protons from specific known states in $^{13}$N. The $^6$He singles spectra for the $^{40}$Ca, $^{90}$Zr($^7$Li, $^6$He) reactions obtained at zero degrees are displayed in Fig. 1, as well as the spectra of $^6$He detected in coincidence with all protons observed in the charged particle array. These latter spectra show only true events. The yields were corrected for random coincidences by setting gates on the ''true+random'' and ''random'' channels in the time spectrum. The time difference between a $^6$He detected in the focal plane and a proton detected in the silicon array, appropriately delayed, was recorded event by event and used to make a coincident time spectrum for each silicon proton detector. The excitation energies corresponding to the proton and neutron emission thresholds ($B_p = 1.08$ and 5.15 MeV; $B_n = 16.29$ and 12.06 MeV, for the $^{40}$Ca and $^{90}$Zr targets, respectively) are indicated in the figure by arrows.

## III. THEORETICAL CALCULATIONS

As mentioned in the Introduction, the inclusive spectrum can contain events from both breakup processes and transfer to resonance states in the intermediate nucleus. In order to separate these processes, the protons emitted from the unbound region of the intermediate nucleus were measured in coincidence with $^6$He particles detected at zero degrees. The energy spectrum of these emitted protons gives the excited energy spectrum of the final nucleus, which in this case is also the target nucleus.

For a given event, the excitation energy of the final nucleus after the emission of a single proton ($E_f$) is determined using the equation

$$E_f = E_x - E_p(m_f + m_p)/m_f - S_p, \tag{1}$$

where $E_x$ is the excitation energy of the intermediate nucleus, $E_p$ is the energy of the emitted proton, evaluated in the center-of-mass frame, $S_p$ is the proton separation energy, and $m_f$ and $m_p$ are the masses of the final (target) nucleus and the proton, respectively.

For a selected region of excitation energy $\Delta E_x$ and a region $\Delta E_f$ of the final nucleus spectrum, the angular correlation function can be written as

$$W(\vartheta_{\text{c.m.}}) = N_p(\vartheta) 4\pi / [N_s \cdot \Delta\Omega] \tag{2}$$

where $N_p(\vartheta)$ is the measured number of protons corrected for the ratio of center of mass to laboratory cross section, $N_s$ is the number of singles events in the excitation energy slice $\Delta E_x$, and $\Delta\Omega$ is the solid angle of an individual proton detector. As noted above, the decay of resonance states should be symmetric about 90°. Thus, any asymmetry in the correlation function, particularly an asymmetric increase at forward angles, will indicate the presence of breakup processes contributing to the inclusive spectra. The correlation function given in Eq. (2) can be fitted with a Legendre polynomial series from which the proton multiplicities $M_p$ can be extracted, viz.

$$W(\vartheta_{\text{c.m.}}) = M_p \Sigma a_i P_i(\cos\vartheta_{\text{c.m.}}), \quad (i \text{ even}) \tag{3}$$

where the fitting is made neglecting the forward-angle 32° point. In any particular case, the fitting is done up to a maximum value of the rank of the Legendre polynomial, depending on the spin values. Detailed results for both targets will be discussed in the following sections. For the $^{40}$Ca target, theoretical predictions of the angular correlations were made for two $9/2^+ \rightarrow 0^+$ transitions with the program CORELY [10] in a similar fashion to that described for neutron decay [11,12]. Here, we have not calculated the density matrix, but rather made the simple assumption of a 100% population of the $\pm 3/2$ magnetic substates. The optical potential parameters of Perey [13] were used for the proton-nucleus scattering states.

The probability of statistical proton decay from the excited nucleus to the target nucleus was calculated with CASCADE in a similar manner to Refs. [14–16]. In the CASCADE calculations, the optical model parameters of Perey [13] were used to calculate the proton transmission coefficients. Since CASCADE is based on the statistical decay of a compound nucleus, level schemes of the excited intermediate and daughter nuclei must be input. For $^{41}$Sc, known levels with their spins were used up to 3.9 MeV excitation. The upper limit for the known levels was taken at 1.4 MeV in $^{91}$Nb. For the daughter nuclei, the limits were chosen from the available data. Above these energies, the level density was calculated using the parameters taken from Dilg *et al.* [17]. The spin distribution in the $^{91}$Nb compound nucleus was calculated within the statistical procedure of CASCADE using the internally calculated values for the maximum angular momentum and the diffuseness. For $^{41}$Sc, the angular momentum distribution used was that determined by Kim *et al.* [18] in the $^{40}$Ca($^3$He,$d$) reaction. As a check, the angular momentum values in the compound nucleus were varied over a wide range and the multiplicities calculated by CASCADE were found to be rather insensitive to these values. The standard values of the other parameters were used since the dominant contribution to particle decay arises from the Coulomb and centrifugal barriers.

The mean proton multiplicity has been calculated with a 2 MeV threshold applied to the proton spectra which corresponds to the experimental threshold of the backward-angle detectors (the forward-angle detector, which had a higher threshold, was not included in the experimental analysis). This software threshold is applied to the protons in the center-of-mass frame of the excited nucleus. The calculation takes into account neutron decay, $\gamma$ decay, and the Coulomb barrier. The calculated multiplicities were not very sensitive to the angular momentum distribution of the compound nucleus. The results may be compared directly to the yield for proton decay measured in the coincidence experiment. If the ratio of the measured multiplicity to the calculated one is close to unity, it suggests that the inclusive spectrum is mainly a result of absorption into resonance states. On the other hand, if this same ratio is small, this implies that the inclusive spectrum has a substantial contribution from breakup processes.

## IV. RESULTS AND DISCUSSION

### A. $^{40}$Ca($^7$Li, $^6$He+$p$)

The $^6$He singles spectrum from the reaction $^{40}$Ca($^7$Li, $^6$He)$^{41}$Sc obtained at zero degrees is shown in Fig. 1(a). Two states are seen to be strongly excited in $^{41}$Sc, the ground state ($7/2^-$) and an excited $9/2^+$ state near 5 MeV. Between 6 and 20 MeV excitation energy, no other prominent peaks are observed although there is an indication of structure at excitation energies near 9 and 11 MeV. This singles spectrum is quite similar to the spectra observed in both the $^{40}$Ca($^{13}$C, $^{12}$B)$^{41}$Sc [19] and $^{40}$Ca($^3$He, $d$)$^{41}$Sc [20] reactions. Both of these reactions show similar strong excitation of the $1f_{7/2}$ ground state and a $1g_{9/2}$ state at 5.04 MeV. The ($^3$He, $d$) experiment at 240 MeV bombarding energy also observed additional $1g_{9/2}$ strength between 8 and 12 MeV excitation energy in $^{41}$Sc. The small structures observed in the same region in the present experiment probably arise from population of this $1g_{9/2}$ strength.

A spectrum of $^6$He in coincidence with all protons detected in the charged particle array is shown in Fig. 1(b). Accidentals have been subtracted. The proton-emission threshold in $^{41}$Sc is 1.09 MeV, but, as described in Sec. III, a software threshold of 2.0 MeV has been applied. The 5.04 MeV peak, corresponding to the $g_{9/2}$ state is clearly seen. There is also structure observed near 9 and 11 MeV, more clearly than in the singles spectrum. There does not appear to be any dramatic decrease in the coincidence spectrum near the neutron threshold of 16.15 MeV, presumably because by then the contribution from two-proton decay is beginning to take effect. Although the two-proton decay threshold is 9.41 MeV, both the proton energies need to be high to have a reasonable probability of decay through the Coulomb barrier. Two-proton decay to $^{39}$K may account for the rise in the coincidence spectrum around 17 MeV of excitation in $^{41}$Sc.

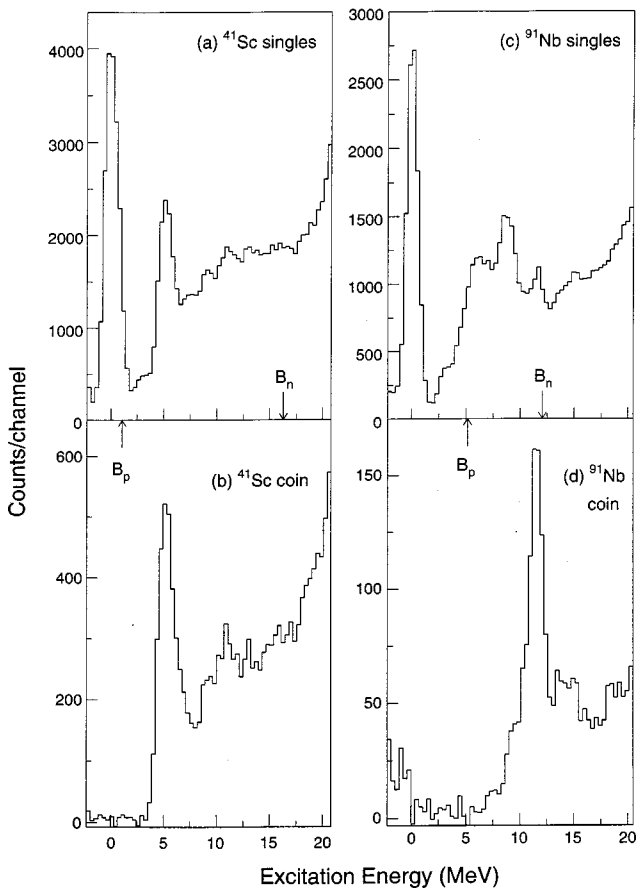


FIG. 1. Singles (top panel) and coincidence (bottom panel) spectra for the ($^7$Li, $^6$He) reaction at 50 MeV/nucleon on targets of $^{40}$Ca and $^{90}$Zr. Arrows indicate the proton and neutron emission thresholds in each case.

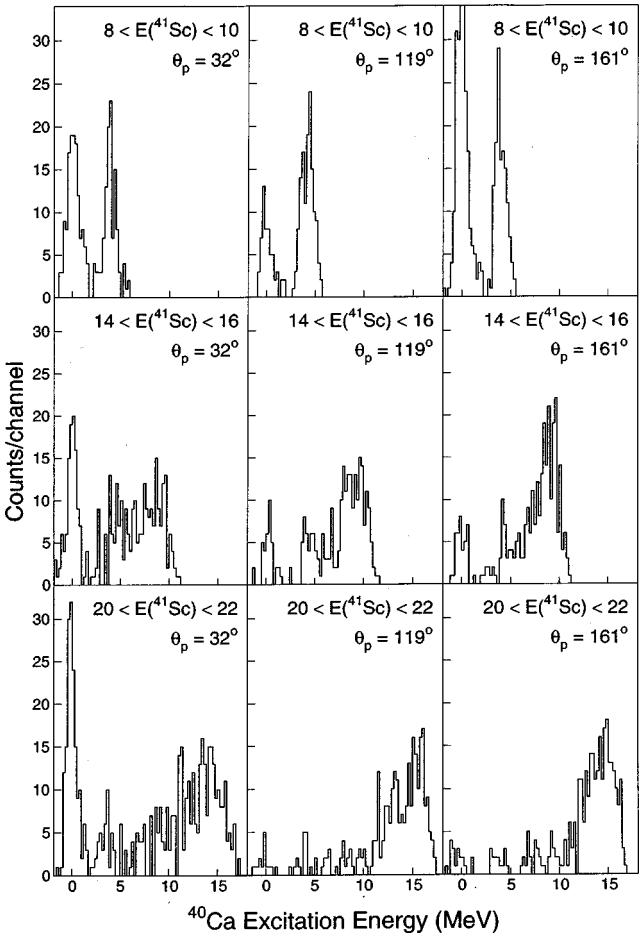


FIG. 2. Spectra of $E_f$ for $^{40}$Ca constructed from various 2-MeV slices in excitation energy of $^{41}$Sc (as noted on each plot) at laboratory angles of 32°, 119°, and 161°.

The final excitation energy in $^{40}$Ca was calculated from the decay proton energies as described in Sec. III. Figure 2 shows examples of final energy spectra for three different excitation energy regions in $^{41}$Sc ($9\pm1$ MeV, $15\pm1$ MeV, and $21\pm1$ MeV), each at three angles. At the most forward angle of 32°, decay to the ground state is observed strongly even at the highest excitation energy. At backward angles (119° and 161°), the ground state and a few low-lying states are observed in $^{40}$Ca for decay from the 8–10 MeV excitation energy region in the intermediate nucleus $^{41}$Sc. However, at higher excitation energies in $^{41}$Sc, the decay to the ground state and low-lying states in $^{40}$Ca is much weaker and the predominant decay is to high-lying states in $^{40}$Ca. This is similar to the results obtained for neutron decay following neutron stripping on $^{64}$Ni, $^{90}$Zr, and $^{120}$Sn [11].

Some representative angular distributions for decays to 5 MeV wide regions of excitation energy in the final nucleus, $^{40}$Ca, are shown in Fig. 3. For certain cases where the proton energy is 4 MeV or less, only a lower limit could be obtained for the cross section at 32°, because of the relatively high threshold on this detector (note that the 32° data were not used in further analysis). The angular distributions for the lower excitation energy regions of the intermediate nucleus $^{41}$Sc, which decay to the ground state of $^{40}$Ca, are peaked in the backward direction. However, as the excitation energy in $^{41}$Sc increases the angular distributions for ground-state decay become isotropic except for the most forward angle. The increase of the cross section at forward angles is presumably caused by breakup of the incident $^7$Li projectile, the yield of which tends to be greatest near the beam direction. For decays to higher excitation energy regions in the final nucleus $^{40}$Ca, the angular distributions are quite isotropic for all excitation energy regions of the intermediate nucleus, $^{41}$Sc. Two of the experimental angular distributions from the 5 and 9 MeV regions of $^{41}$Sc are compared with calculations from CORELY as described in Sec. III. These calculations assume decay of a $9/2^+$ state to the $0^+$ ground state of $^{40}$Ca and are in reasonably good agreement with the measured angular distributions of the emitted protons.

Figure 4 (upper panel) shows a spectrum of $E_f$, determined from Eq. (1) for all backward-angle coincidence events. The ground state of $^{40}$Ca is populated quite strongly. The next most prominent feature is the peak near 4 MeV, which probably has components corresponding to the $3^-$ state at 3.74 MeV as well as the $2^+$ state at 3.90 MeV and the $5^-$ state at 4.5 MeV. Higher states in $^{40}$Ca up to 15 MeV excitation energy are also populated. CASCADE calculations, normalized to the experimental data at excitation energies

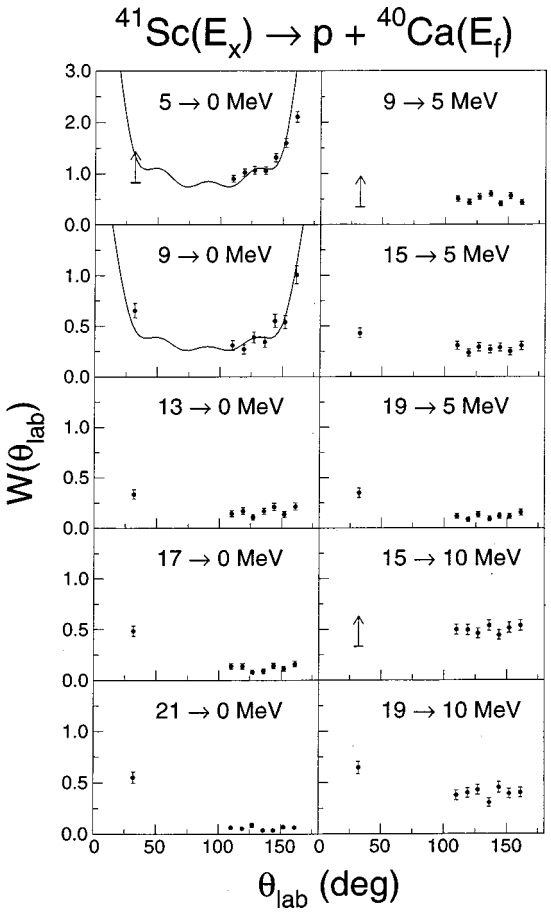


FIG. 3. Angular correlations $W(\theta)$ for $^{41}Sc \rightarrow {}^{40}Ca + p$, plotted as a function of proton laboratory angle. The specific mean excitation energy in the initial ($E_x$) and final ($E_f$) nuclei are given on each plot in MeV. The bar on the vertical arrow at 32° for certain cases represents a lower limit, as explained in the text. The curves are CORELY predictions, normalized to the data.

above 10 MeV, are shown as a solid line in the same figure. The CASCADE predictions are significantly lower than the population of the low-lying states, particularly of the ground state where the ratio of observed to predicted strength is more than a factor of 3. This indicates that there is significant direct decay from the highly excited states in $^{41}Sc$ to the ground state of $^{40}Ca$ and to the low-lying states around 4 MeV.

The measured proton multiplicity was obtained as described in Sec. III and is compared with the results of a CASCADE calculation in Fig. 5 (upper panel). The calculated multiplicity rises quite rapidly above 14 MeV excitation energy as the proton energies from the $(p,2p)$ channel (threshold 9.42 MeV) exceed the Coulomb and centrifugal barriers. However, no corresponding increase is observed in the measured multiplicity. At 20 MeV excitation energy, the calculated multiplicity is roughly 50% larger than the measured multiplicity implying that about one third of the inclusive spectrum arises from breakup processes at excitation energies between 14 and 22 MeV. This conclusion is rather independent of the parameters of the model since once the proton energies significantly exceed the Coulomb and centrifugal barriers, the states must decay.

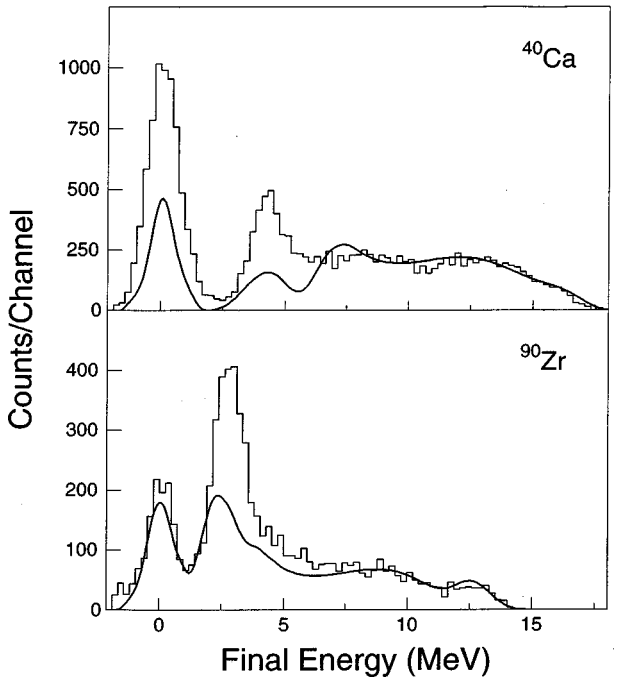


FIG. 4. Composite spectra of the final energy ($E_f$) in $^{40}Ca$ and $^{90}Zr$ for all backward angle detectors. The solid lines are the CASCADE predictions described in the text.

### B. $^{90}Zr(^{7}Li, {}^{6}He+p)$

The $^{6}He$ spectrum from the reaction $^{90}Zr(^{7}Li, {}^{6}He)^{91}Nb$ obtained at zero degrees is shown in Fig. 1(c). The ground state ($9/2^{+}$) is strongly excited, which agrees with the predicted favorable angular momentum matching for an $l=4$ transfer [21]. Broad peaks are observed at excitation energies of 6.1 and 9.2 MeV. Similar features were observed in data for the same reaction at a bombarding energy of 30 MeV/nucleon [7]. A small sharp peak is observed near 12 MeV. This appears to correspond to the excitation of one or more of the three isobaric analog states (IAS) observed at 11.93, 12.07, and 12.15 MeV by Finkel *et al.* [22]. The 12 MeV state observed in the present experiment is likely to be a high-spin state, either $7/2^{+}$ or $11/2^{-}$, both of which are anticipated in this region. The other IAS observed in Ref. [22] at 9.86 MeV ($5/2^{+}$) and 13.38 MeV ($7/2^{+}$) do not appear to be strongly excited in the present reaction, although one cannot rule out the 9.86 MeV state being obscured by the broad state near 9.2 MeV.

Proton emission is expected to be dominant up to the neutron threshold of 12.06 MeV. However, due to the strong Coulomb and centrifugal barriers, proton emission is strongly suppressed below 9 MeV. Hence, the strong peaks seen near 6.5 and 9.0 MeV in the singles spectrum are not seen in the coincidence spectrum [see Fig. 1(d)]. This difference is confirmed by the CASCADE calculations, which predict that proton decay is strongly suppressed in this region. The IAS near 12 MeV show up much more strongly in the coincidence spectrum than in the singles spectrum.

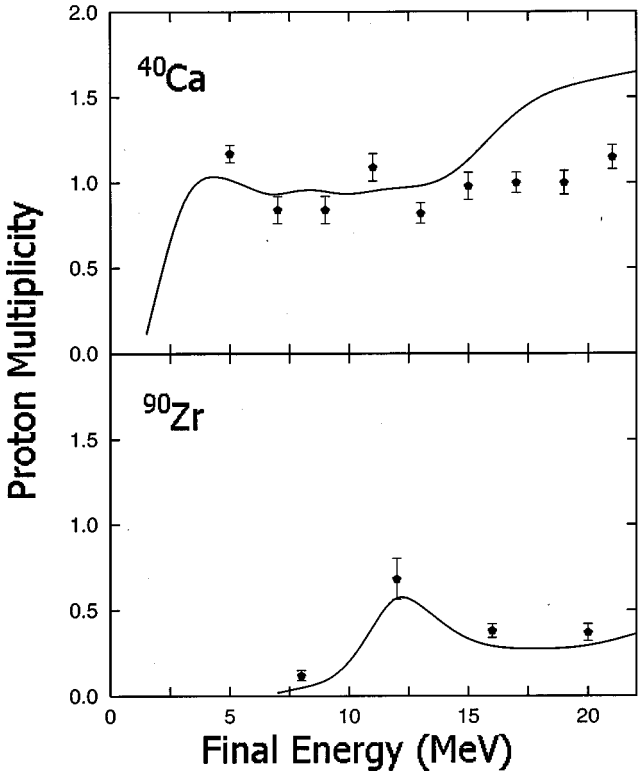


FIG. 5. Experimental proton multiplicities (points) and corresponding CASCADE calculations (solid lines) plotted against final energy ($E_f$) for the $^{40}$Ca and $^{90}$Zr targets.

Excitation energy ($E_f$) spectra of $^{90}$Zr from the proton decay of $^{91}$Nb were obtained as described in Sec. III and some examples are shown in Fig. 6. In order to obtain sufficient statistics in this case, the width of the energy slice in the intermediate nucleus was 4 MeV. The ground state of $^{90}$Zr is not strongly excited but there is significant strength observed in the region around 3 MeV in $^{90}$Zr. This strength arises from decay of the 12 MeV excitation energy region of $^{91}$Nb. The 3 MeV region of excitation energy in $^{90}$Zr contains a $5^-$ state at 2.3 MeV, a $3^-$ state at 2.7 MeV, a $4^+$ state at 3.1 MeV, and a $6^+$ state at 3.4 MeV. From the centroid of the peak, and that of the corresponding peak in the coincidence spectrum (see below), it appears that there is significant excitation of the $3^-$ state, although the resolution of the present experiment is not sufficient to resolve the specific states. For higher excitation energies in $^{91}$Nb the decay is predominantly by emission of low-energy protons implying mainly a statistical process. We note that the threshold for two-proton emission in $^{91}$Nb is 13.54 MeV, and the requirement that both protons escape through the Coulomb barrier means that two-proton emission will not be significant below about 21 MeV of excitation.

For all backward angle coincidence events, $E_f$ is calculated and the resulting spectrum is displayed in Fig. 4 (lower panel). The ground state of $^{90}$Zr is populated fairly strongly, although not as strongly as the region between 2 and 4 MeV. The centroid of this peak is at 2.7 MeV, suggesting that the main contribution is from the $3^-$ state, as discussed above.

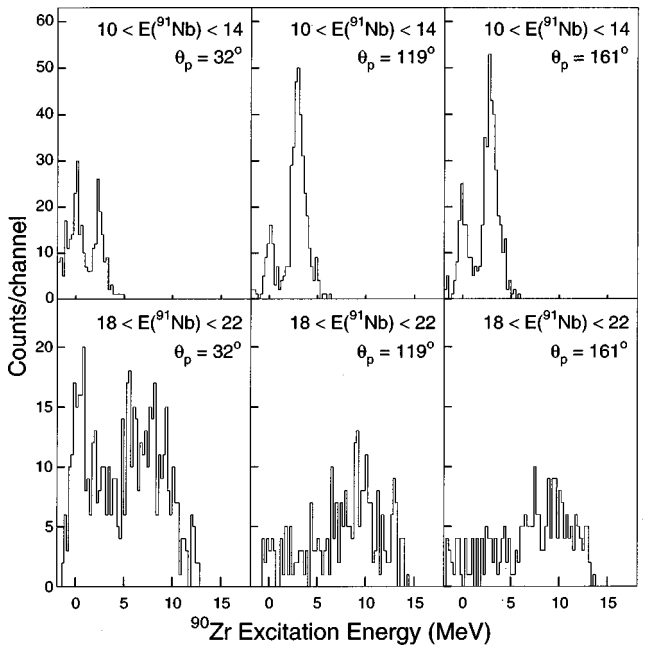


FIG. 6. Spectra of $E_f$ for $^{90}$Zr constructed from 4-MeV slices in excitation energy of $^{91}$Nb at laboratory angles of 32°, 119°, and 161°.

The CASCADE calculations are normalized to the experimental data at excitation energies around 10 MeV and are shown as a solid line in the same figure. The CASCADE calculations predict most of the spectrum of $^{90}$Zr quite well including the ground-state strength. The notable exception is the experimentally strong yield to the 3 MeV region. This strength likely arises from the direct decay of one or more of the IAS near 12 MeV by a direct nonstatistical process. With somewhat better resolution more definitive information could be obtained on this transition.

Some examples of angular distributions of various transitions from $^{91}$Nb to $^{90}$Zr are shown in Fig. 7. For the case of $^{91}$Nb(12 MeV) to $^{90}$Zr(3 MeV) where the proton energy is less than 4 MeV, only a lower limit could be obtained for the cross section at 32°, because of the relatively high threshold on this detector. The angular distributions are all quite isotropic except for the 32° point, for which, apart from the case mentioned above, the cross section is slightly higher than that of the backward-angle points. Again this may be the residue of breakup effects and so this angle was neglected in further analysis. There is a slight increase towards backward angles in the case of the fairly weak transition from the 12 MeV region to the ground state of $^{90}$Zr. The angular distribution for the decay of the 12 MeV region to the region around 3 MeV is quite flat, presumably because of the large number of possible $l$ values for the decay protons.

The proton multiplicity was determined as a function of excitation energy as described in Sec. III. Figure 5 (lower panel) compares the multiplicity as a function of excitation energy in $^{91}$Nb. In this case, there is good agreement between the experimental results and the CASCADE calculations throughout the measured $E_f$ spectrum. This suggests that most of the observed strength, at least up to 20 MeV excitation energy, is due to proton decay from the compound

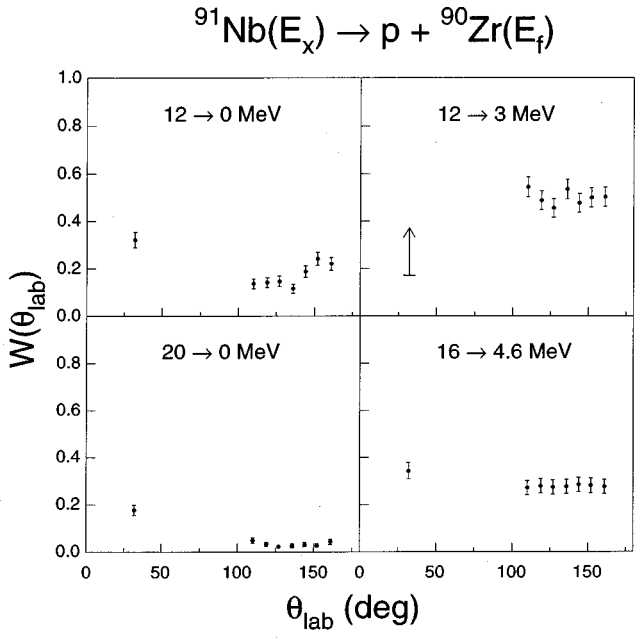


FIG. 7. Angular correlations $W(\theta)$ for $^{91}\mathrm{Nb}\rightarrow{}^{90}\mathrm{Zr}+p$, plotted as a function of proton laboratory angle. The mean excitation energy in the initial ($E_x$) and final ($E_f$) nuclei are given on each plot in MeV. The bar on the vertical arrow at 32° for $^{91}$Nb(12 MeV) to $^{90}$Zr(3 MeV) represents a lower limit, as explained in the text.

nucleus or resonance states formed in the transfer process and not from breakup.

## V. CONCLUSIONS

Proton decay following the proton transfer reaction ($^{7}$Li, $^{6}$He) on targets of $^{40}$Ca and $^{90}$Zr was measured at 50 MeV/nucleon bombarding energy in order to investigate the source of the underlying continuum observed in this and many other stripping reactions. By measuring the coincident protons at backward angles, we are able to eliminate the contribution of elastic breakup. The angular distributions of the emitted protons were measured for slices of excitation energy in the intermediate nucleus and compared to predictions, from which the proton multiplicities were extracted. These proton multiplicities were compared with the proton multiplicity calculated by the program CASCADE. In addition, the decay spectra were compared to CASCADE calculations and the amount of direct decay was therefore determined.

In the case of the $^{40}$Ca target, there is reasonable agreement between the measured multiplicities and the predictions of CASCADE up to an excitation energy of 14 MeV in $^{41}$Sc. This implies that in this energy region the singles spectrum arises predominantly (about 70%) from compound or resonance states and that there is very little contribution to the singles spectrum from breakup processes. At higher excitation energies, the calculated multiplicities are higher than the measured ones implying that there is an increased contribution from breakup. However, even up to 20 MeV there is still a very significant contribution from resonant states. There is significant direct decay observed to the ground state and to states near 4 MeV in $^{40}$Ca.

The situation is somewhat more complicated in the case of the $^{90}$Zr target. The cross section for the proton decay obtained from the transfer cross section and the proton decay probability agreed well with the data at low excitation energy in $^{91}$Nb. However, the statistical calculations of CASCADE do not take into account the direct decay of the IAS observed near $E_f = 12$ MeV. In addition the onset of neutron emission lies in the same position as the strongly excited IAS. Nevertheless, the CASCADE multiplicity predictions follow the rise and fall of the data in this region. Even at higher excitation energies, there is reasonable agreement with the CASCADE calculation, which implies that there is substantial sequential decay taking place.

## ACKNOWLEDGMENTS

This work was supported in part by the U.S. NSF under Grants No. PHY89-13815 and INT-9217404, and by the Centre National de la Recherche Scientifique (CNRS, France). The authors also wish to thank Angela Bonaccorso and Alexander Sakharuk for valuable discussions.

[1] S. Galès, Ch. Stoyanov, and A. I. Vdovin, Phys. Rep. **166**, 125 (1988).
[2] A. Bonaccorso, D. M. Brink, and L. Lo Monaco, J. Phys. G **13**, 1407 (1987).
[3] A. Bonaccorso and D. M. Brink, Phys. Rev. C **38**, 1776 (1988).
[4] A. Bonaccorso and D. M. Brink, Phys. Rev. C **46**, 700 (1992).
[5] A. Bonaccorso, Phys. Rev. C **51**, 822 (1995).
[6] I. Lhenry *et al.*, Phys. Rev. C **54**, 593 (1996).
[7] G. H. Yoo, G. M. Crawley, N. A. Orr, J. S. Winfield, J. E. Finck, S. Galès, Ph. Chomaz, I. Lhenry, and T. Suomijärvi, Phys. Rev. C **47**, 1200 (1993).
[8] B. M. Sherrill, D. J. Morrissey, J. A. Nolen, Jr., and J. A. Winger, Nucl. Instrum. Methods Phys. Res. B **56**, 1106 (1991).
[9] F. Puhlhofer, Nucl. Phys. **A280**, 267 (1970); M. N. Harakeh, modified program CASCADE (unpublished).
[10] J. Van de Wiele, program CORELY (unpublished).
[11] S. Fortier *et al.*, Phys. Rev. C **52**, 2401 (1995).
[12] H. Laurent *et al.*, Phys. Rev. C **52**, 3066 (1995).
[13] F. G. Perey, Phys. Rev. **131**, 745 (1963).
[14] H. Hashim and D. M. Brink, Nucl. Phys. **A476**, 107 (1988).
[15] C. Mahaux and R. Sartor, Nucl. Phys. **A493**, 157 (1989).
[16] E. Vogt, *Advances in Nuclear Physics*, Vol. 1 (Plenum, New York, 1968), p. 261.
[17] W. Dilg, W. Schantl, H. Vonach, and M. Uhl, Nucl. Phys. **A217**, 269 (1973).
[18] C.-Y. Kim, T. Udagawa, J. Guillot, H. Langevin-Joliot, J. van

de Wiele, J. J. Florent, A. Willis, E. Hourani, E. Gerlic, and G. Duhamel-Chretien, Phys. Rev. C **50**, 2035 (1994).
[19] M. Braeunig *et al.*, Nucl. Phys. **A519**, 631 (1990).
[20] J. Guillot, H. Langevin-Joliot, J. van de Wiele, E. Gerlic, J. J. Florent, A. Willis, G. Duhamel-Chretien, and E. Hourani, Phys. Lett. B **258**, 271 (1991).
[21] N. Anyas-Weiss *et al.*, Phys. Rep., Phys. Lett. **12C**, 201 (1974).
[22] G. Finkel, D. Ashery, A. I. Yavin, A. Boudard, G. Brug, A. Chaumeaux, and M. Rouger, Phys. Rev. C **19**, 1782 (1979).